2014

Direct synthesis of RGO/Cu2O composite films on Cu foil for supercapacitors

Xiangmao Dong
East China University of Science and Technology

Kun Wang
Jiangsu University

Chongjun Zhao
University of Wollongong, chongjunzhao@ecust.edu.cn

Xiuzhen Qian
East China University of Science and Technology

Shi Chen
Wuhan University of Technology

See next page for additional authors

Publication Details

Dong, X., Wang, K., Zhao, C., Qian, X., Chen, S., Li, Z., Liu, H. & Dou, S. (2014). Direct synthesis of RGO/Cu2O composite films on Cu foil for supercapacitors. Journal of Alloys and Compounds, 586 745-753.

Direct synthesis of RGO/Cu2O composite films on Cu foil for supercapacitors

Abstract
Reduced graphene oxide/cuprous oxide (RGO/Cu2O) composite films were directly synthesized on the surface of copper foil substrates through a straight redox reaction between GO and Cu foil via a hydrothermal approach. Characterization of the resultant composites with X-ray diffraction, Raman spectroscopy, X-ray photoelectron spectroscopy, and field emission scanning electron microscope (FESEM) confirms the formation of Cu2O and reduction of GO, in which Cu2O nanoparticles were well covered by RGO. The resultant composites (referred to as RGO/Cu2O/Cu) were directly used as electrodes for supercapacitors, and their electrochemical performance was assessed by cyclic voltammetry (CV), galvanostatic charge–discharge (GCD), and electrochemical impedance spectrometry (EIS) in 1 M KOH aqueous solution. A specific capacitance of 98.5 F g−1 at 1 A g−1 was obtained, which is much higher than that of pure Cu2O prepared under the same conditions, due to the presence of RGO.

Keywords
supercapacitors, synthesis, rgo, cu2o, composite, films, cu, foil, direct

Disciplines
Engineering | Physical Sciences and Mathematics

Publication Details
Dong, X., Wang, K., Zhao, C., Qian, X., Chen, S., Li, Z., Liu, H. & Dou, S. (2014). Direct synthesis of RGO/Cu2O composite films on Cu foil for supercapacitors. Journal of Alloys and Compounds, 586 745-753.

Authors
Xiangmao Dong, Kun Wang, Chongjun Zhao, Xiuzhen Qian, Shi Chen, Zhen Li, Hua-Kun Liu, and S X. Dou

Direct synthesis of RGO/Cu_2O composite films on Cu foil for supercapacitors

Xiangmao Dong[a], Kun Wang[a], Chongjun Zhao*[a,b], Xiuzhen Qian[a], Shi Chen*[c], Zhen Li*[b], Huakun Liu[b], Shixue Dou[b]

[a]*Key Laboratory for Ultrafine Materials of the Ministry of Education, Shanghai Key Laboratory of Advanced Polymeric Materials, School of Materials Science and Engineering, East China University of Science and Technology, Shanghai 200237, P.R. ChinaTel: +86-21-6425 0838; Fax: +86-21-6425 0838; E-mail: chongjunzhao@ecust.edu.cn*

[b]*Institute for Superconducting and Electronic Materials, University of Wollongong, Wollongong 2500, Australia. Tel: +61-2-4221-5163; Fax: +61-2-4221-5731; E-mail: zhenl@uow.edu.au*

[c]*School of Information Engineering, Wuhan University of Technology, Wuhan, 430070*

ABSTRACT

Reduced graphene oxide/cuprous oxide (RGO/Cu_2O) composite films were directly synthesized on the surface of copper foil substrates through a straight redox reaction between GO and Cu foil via a hydrothermal approach. Characterization of the resultant composites with X-ray diffraction, Raman spectroscopy, X-ray photoelectron spectroscopy, and field emission scanning electron microscope (FESEM) confirms the formation of Cu_2O and reduction of GO, in which Cu_2O nanoparticles were well covered by RGO. The resultant composites (referred to as RGO/Cu_2O/Cu) were directly used as electrodes for supercapacitors, and their electrochemical performance was assessed by cyclic voltammetry (CV), galvanostatic charge-discharge (GCD), and electrochemical impedance spectrometry (EIS) in 1 M KOH aqueous solution. A specific capacitance of 98.5 F g^{-1} at 1 A g^{-1} was obtained, which is much higher than that of pure Cu_2O prepared under the same conditions, due to the presence of RGO.

***Keywords**:* RGO/Cu_2O/Cu composites; Thin films; Hydrothermal synthesis; Supercapacitors

1. Introduction

Over the past several decades, supercapacitors (also called electrochemical capacitors) have been attracting considerable attention due to their higher power density, shorter charging time, higher cycling efficiency, and longer lifetime in comparison with batteries [1-5]. They also have higher energy density than conventional dielectric capacitors. Therefore, supercapacitors are one of the most promising energy storage devices and power suppliers for digital products, hybrid-electric vehicles, and other portable electronic devices [6]. Their energy density (0.5-10 W h kg^{-1}) is still lower than that of batteries, however, and many efforts have been made to improve it to the point of being at least comparable to that of batteries. One efficient approach is the use of electrode materials which have a similar battery-type Faradaic current profile. Certain metal oxides and hydroxides, especially transition metal oxides or hydroxides, and organic materials, including conducting polymers, can meet this requirement and serve as electrode materials for supercapacitors. One promising candidate is RuO_2, and the fabricated supercapacitors have a specific capacitance of 1340 F g^{-1} and a specific energy of 7.5 W h kg^{-1} [7, 8]. RuO_2 is very expensive [8, 9], however, and the use of cost-effective transition metal oxides such as MnO_2, SnO_2, TiO_2 and $Ni(OH)_2$ as alternatives has been investigated [10-13]. Most pure metal oxides or hydroxides suffer from some intrinsic disadvantages, however, such as mechanical brittleness, chemical instability, and low conductivity, which limit their application in flexible electrochemical energy storage devices [14, 15].

The above disadvantages of metal oxides or hydroxides could be overcome by combining them with versatile graphene to form composites, as graphene is a two-dimensional (2D) material with extraordinary electrical, and mechanical properties [16], large surface area and high chemical stability. On the one hand, the high mechanical elasticity of graphene (elastic modulus is about 1 TPa) [17], which has been used in the fields of nanoelectronics and spintronics, can improve the flexibility of composites [18, 19]. The intrinsic high electrical conductivity (2420 S m^{-1}) and large specific surface area (2630 m^2 g^{-1}) of graphene could endow supercapacitors with high specific power [14, 18]. On the other hand, metal oxide (or metal hydroxide) nanoparticles could act as spacers in the interlayers of graphene sheets to prevent them from aggregation, increasing the interplanar spacing and contact area with the electrolyte [20].

Up to now, some transition metal oxides, hydroxides (including those with variable valence), and their composites with graphene have been widely used in energy storage. Among the transition metal oxides, Cu_2O (or CuO) as an abundant metal oxide has been investigated as an electrode material for Li ion batteries (LIBs) [21], due to its high theoretical capacity, low cost, and environmental friendliness. Copper oxide composites with graphene have been also used in LIBs [22-34]. Their application in batteries suggests the feasibility of their application in supercapacitors, as similar Faradaic redox reactions to those in LIBs are also used in supercapacitors. There are only a few reports on this aspect [35-37], however, in which reduced graphene oxide/cuprous oxide (RGO/Cu_2O) composites were usually prepared from

copper salts with graphene oxide [33-35, 38, 39], and the resultant RGO/Cu_2O or RGO/CuO powder has to be carefully washed due to the presence of residual cations. This rinsing process can be omitted when elemental Cu is used as the Cu source for RGO/Cu_2O composites, because Cu can be oxidized into Cu_2O or CuO, and GO can be reduced to RGO. There is no other by-product formed.

Herein, we directly synthesized RGO/Cu_2O nanocomposite films on Cu foil substrates through a hydrothermal process, in which the formation of Cu_2O nanoparticles (NPs) and the reduction of GO simultaneously took place in an one-pot reaction, and the formed Cu_2O NPs were covered with reduced graphene oxide (RGO) sheets. The resultant sandwich composites (i.e. RGO/Cu_2O/Cu) were then used as electrodes in supercapacitors, and showed excellent electrochemical performance due to their unique structure, in which Cu_2O nanoparticles formed in-situ on the surface of Cu foil. The reduced graphene oxide notably improved the capacity of the RGO/Cu_2O/Cu electrodes.

2. Experimental

2.1. Materials and reagents

Pristine graphite powder, hydrochloric acid (HCl, 36.0–38.0wt%), hydrogen peroxide (H_2O_2, 30wt%), sulfuric acid (H_2SO_4, 95–98wt%), potassium permanganate ($KMnO_4$), phosphorus pentoxide (P_2O_5), potassium persulfate ($K_2S_2O_8$) and ethanol (C_2H_5OH, >99.7wt%) were obtained from the Shanghai Chemical Company. Copper substrates were obtained from Alfa Aesar. All chemical reagents were used as

received without any further purification. Water used in all syntheses was distilled and deionized.

2.2. Preparation of graphene oxide

GO was synthesized by a modified Hummer's method [40, 41]. Briefly, graphite powder (3 g, 325 mesh) was put into an 80 °C solution of concentrated H_2SO_4 (12 mL), $K_2S_2O_8$ (2.5 g), and P_2O_5 (2.5 g). The mixture was kept at 80 °C for 4.5 h. Then, the mixture was diluted with 500 mL of de-ionized (DI) water and left overnight. The mixture was filtered and washed with water to remove the residual acid. The product was dried under ambient conditions overnight.

Pre-oxidized graphite powder was added into cold (0 °C) concentrated H_2SO_4 (120 mL). Then, $KMnO_4$ (15 g) was slowly added, with the temperature of mixture kept below 20 °C. After addition of 250 mL of water, the mixture was stirred for 2 h, and then an additional 700 mL of water was added. After that, 20 mL of 30% H_2O_2 was added into the mixture, and the solution changed into brilliant yellow, accompanied by the generation of bubbles. The mixture was filtered and washed with diluted HCl aqueous solution (10wt%, 1 L) to remove metal ions. The brownish yellow solution was centrifuged at 10000 rpm, the supernatant solution was decanted away, and the resulting material was subjected to multiple washings with water until the pH was 7. The obtained GO was dispersed in a certain amount of water.

2.3. Preparation of RGO/Cu_2O composites on copper sheets

In a typical procedure, highly pure copper substrates (99.99%) were carefully cleaned with acetone, ethanol, and water, respectively, in an ultrasound bath to

remove surface impurities. The as-synthesized GO (30 mg), which was dispersed in deionized water (50 ml), was sonicated for 1 h. Cleaned copper foil substrates (1×2 cm^2) were put into the above GO solution and stirred for 1 h. The mixture was loaded into a 100 ml Teflon-lined stainless steel autoclave for hydrothermal reaction at a selected temperature for 24 h. The final product was washed with ethanol and water, and dried in an oven at 60 °C for 12 h. In order to study the effects of temperature on the formation of the RGO/Cu_2O composites, a series of samples were prepared at 160 °C, 180 °C, 200 °C, 220 °C, and 240 °C, respectively, which were designated as RGO/Cu_2O/Cu-160, RGO/Cu_2O/Cu-180, RGO/Cu_2O/Cu-200, RGO/Cu_2O/Cu-220, and RGO/Cu_2O/Cu-240, according to the preparation temperature. In the absence of copper or GO, Cu_2O/Cu-200 films and RGO powder were obtained via a similar process at 200 °C.

2.4. Characterizations

Wide-angle (10°–80°) powder X-ray diffraction (XRD) was carried out using a polycrystalline X-ray diffractometer (RIGAKU, D/MAX 2550 VB/PC, 40 kV/200 mA, $\lambda\alpha_1$ = 1.5406 Å) at room temperature. Fourier transform infrared (FTIR) spectra were collected on a NICOLET 6700 FTIR spectrophotometer. To demonstrate the particle uniformity and morphology, all samples were examined by field emission scanning electron microscopy (FESEM) using a JEOL SM-6360LV microscope. Raman spectra were collected on an INVIA Raman microprobe (Renishaw Instruments, England) with 514 nm laser excitation. X-ray photoelectron spectroscopy (XPS) measurements were performed on a Perkin-Elmer PHI5000CESCA system

with a base pressure of 10^{-9} Torr.

2.5. Electrochemical measurements

RGO/Cu_2O/Cu composites were dried under vacuum at 60 °C for 12 h, and then directly used as working electrodes, with each having an area of 1×1 cm^2. The electrolyte was 1 M KOH aqueous solution. Three-electrode cells were constructed consisting of an as-fabricated working electrode, a counter electrode (Pt foil, 2×3 cm^2), and a reference saturated calomel electrode (SCE). The capacitive performances of all electrodes were evaluated with an electrochemical work-station (CHI660E, Shanghai) using cyclic voltammetry, chronopotentiometry, and AC impedance tests. After the performance tests were finished, the RGO/Cu_2O/Cu electrodes were sonicated for 30 min, and then subjected to hydrochloric acid (10% wt.) and sonicated for another 10 min. Thus, the loading amount of RGO/Cu_2O was determined from the weight difference of the electrodes before testing and after ultrasonication, which was controlled at about 2 mg.

3. Results and discussion

The obtained RGO/Cu_2O/Cu composites were characterized with state-of-the-art facilities. Fig.1 shows the X-ray diffraction (XRD) patterns of the bare Cu foil substrates, the RGO powder, and the RGO/Cu_2O/Cu composites prepared at different temperatures, respectively. Three peaks centered at 43.2°, 50.4°, and 73.4°, assigned to the (111), (200), and (220) planes of metallic copper [42], can be clearly observed in the patterns of the copper foil and the RGO/Cu_2O/Cu composites. The presence of

Cu diffraction peaks in the composites suggests that the Cu foil substrates were not entirely used up in these samples. Five new characteristic diffraction peaks at 29.3°, 36.2°, 42°, 61.1°, and 73.9° in the composites correspond to the (110), (111), (200), (220), and (311) crystalline planes of cubic Cu_2O, respectively (JCDS 78–2076) [43]. In addition, the relative intensity of the strongest diffraction peak of Cu_2O (i.e., (111) at $2\theta = 36.2°$) increases with increasing temperature. These results indicate the formation of cubic Cu_2O particles on the surface of the Cu foil after the hydrothermal treatment, and their crystallinity increases with increasing temperature. It should be noted that the broad peak of RGO at 23.7° is negligible, due to the strong peaks of Cu and Cu_2O.

The formation of Cu_2O indicated by the XRD results suggests the occurrence of redox reactions, which can be reflected by the change in the molecular vibrations in the reagents and products. Fig.2 compares the FTIR spectra of the RGO/Cu_2O composite films with that of GO. The GO spectrum shows the presence of various oxygen-containing groups. The peaks at 1701 cm^{-1} , 1219 cm^{-1}, and 1049 cm^{-1} are assigned to C=O, C-O, and C–O–C vibrations, respectively. The peak at 1621 cm^{-1} is due to the skeletal vibration of un-oxidized graphitic domains or the remaining sp^2 carbon character of graphite [44]. Most contributions from oxygen-containing groups decrease or disappear after hydrothermal treatment, which demonstrates that GO has been reduced by the Cu foil. In addition, the characteristic peak of the copper–oxygen stretching vibration in the Cu_2O is observed at 624 cm^{-1} [45, 46].

In order to further prove the reduction of GO during hydrothermal treatment,

Raman spectroscopy was used to characterize these samples (Fig.3). The ratio of the D band (~1350 cm^{-1}), originating from disorder-activated Raman mode, to the G band (~1596 cm^{-1}), corresponding to sp^2 hybridized carbon, is usually used to semi-quantitatively determine the extent of reduction [47]. The slight increase in the D/G ratio from 0.89 (GO) to 0.95 (RGO) suggests a decrease in the average size of the sp^2 domains upon reduction. This means that RGO has a small size and a large quantity of edges, which act as defects and lead to the increase in the D band [48]. Compared with pure RGO, higher D/G ratios are obtained for the composites, i.e. RGO/Cu_2O/Cu-160 (1.18), RGO/Cu_2O/Cu-180 (1.25), RGO/Cu_2O/Cu-200 (1.16), RGO/Cu_2O/Cu-220 (1.11), and RGO/Cu_2O/Cu-240 (1.22), indicating that RGO was deeply reduced to form more disordered structure during the hydrothermal process with the assistance of copper [49]. In addition, the peak at 2696 cm^{-1}, corresponding to the overtone of the 2D band, red-shifts to a higher wave number and becomes broader, which indicates the multilayer structure of RGO in the composites [50]. The peak observed at 2932 cm^{-1} is associated with the (D + D') band and attributed to defects [47]. It should be noted that the Raman peaks of Cu_2O in the RGO/Cu_2O/Cu composites were not observed because the internal Cu_2O layer is well covered by the RGO film as shown in the SEM images (Fig.5 and Fig.6).

Fig.4(a-c) shows the C1s spectra of GO, RGO, and RGO/Cu_2O/Cu-200, respectively. They could be deconvoluted into three peaks at 284.78, 286.97, and 288. 77 eV, which are associated with C–C, C–O, and C=O, respectively. The peak intensities of C–O and C=O are much stronger in GO (Fig.4a), but they are drastically

reduced after hydrothermal treatment (Fig.4b). The relative intensity of C=O in the RGO/Cu_2O/Cu-200 is smaller than that in the pure RGO, indicating that a deeper reduction occurred in the presence of copper foil (Fig.4c).

The C/O ratios for these samples are calculated to be 1.54 (GO), 2.87 (RGO), 3.08 (RGO/Cu_2O/Cu-160), 3.56 (RGO/Cu_2O/Cu-180), 2.55 (RGO/Cu_2O/Cu-200), 3.12 (RGO/Cu_2O/Cu-220), and 3.00 (RGO/Cu_2O/Cu-240), respectively (Fig.4d). The results demonstrate the deeper reduction of GO in the composites than in the pure GO, which is consistent with the Raman results.

For Cu foil (Fig.4e, bottom), there are two small peaks at 944.20 and 962.63 eV (marked with arrows) besides the main Cu $2p_{1/2}$ (932.52 eV) and Cu $2p_{3/2}$ (952.53 eV) peaks, which indicates a thin oxide coating on the Cu surface [51]. The Cu 2p of RGO/Cu_2O/Cu-200 (Fig.4e, top) contains two main peaks at 932.95 eV and 952.68 eV, corresponding to the $Cu2p_{3/2}$ and $Cu2p_{1/2}$ peaks of Cu(I) [52, 53] and/or Cu(0), respectively. Similar to the spectrum of Cu foil, a weak Cu(II) signal was detected owing to the oxidation after the exposure of the Cu_2O/RGO sample to air [54]. Although the binding energies of Cu and Cu_2O in the XPS spectra are similar, they can be distinguished from their LMM-2 Auger transitions, as displayed in Fig.4f. The binding energies at 570 eV and 568 eV corresponding to Cu(I) and Cu(0) are clearly distinguished [55].

In the FESEM images of RGO/Cu_2O/Cu-200 (Fig.5a, 5c), spheroidal Cu_2O particles with a size of 200-800 nm that were covered by graphene sheets are clearly observed. Smaller cubic particles (~ 200 nm) on top of big particles were obtained

under the same hydrothermal treatment, however, in the absence of GO (Fig.5b). Therefore, the presence of GO drastically influences the morphology and size of the Cu_2O particles [48], i.e. the particle size increased from 200 nm to ~800 nm, accompanied by a change of shape from spheroidal into cubic. Another reference sample was obtained by the same hydrothermal treatment of GO in the absence of Cu foil (Fig.5d). Aggregated and crumpled RGO sheets formed thick flakes with negligible separation, which is consistent with the previous report [56]. This indicates that the introduction of Cu foil and the formation of Cu_2O efficiently facilitate spreading of the RGO sheets on the surface of the Cu_2O layer, providing a large surface area for electrochemical activities.

Fig.6 shows FESEM images of the RGO/Cu_2O/Cu composites prepared at other temperatures. From their top-view images (Fig.6(a, c, e, g)), there is no obvious difference among them, except for a slight increase in the Cu_2O particle size with increasing temperature. The Cu_2O particles are always covered by the RGO sheets. There is a big difference, however, in the RGO films, which can be observed from their tilted-view images (Fig.6(b, d, f, h)). At low temperature (e.g. 160 °C), the RGO film is very thin and disconnected (forming islands). With the temperature increased from 160 °C to 180 °C, the RGO film becomes slightly thicker, and the RGO sheets connected with each other (Fig.6d). When the temperature reaches 200 °C, a flat net-like structure appears (Fig.5c). A further increase in temperature to 220 °C leads to a broken film due to the formation of large Cu_2O particles. When the temperature further increases to 240 °C, a thick Cu_2O layer forms accompanied by a thin RGO

film. Obviously, a more continuous and thinner RGO is favorable for the transfer of electrons and electrolyte during electrochemical testing [57]. Therefore, the optimum reaction temperature is 200 °C.

On the basis of the above results, we propose the following formation mechanism (Scheme 1). Firstly, Cu foil substrates could react with water under hydrothermal conditions to form Cu(OH) and produce reactive hydrogen (H*) or hydrogen (H_2). Then, both H* and H_2 can reduce the –COOH and –OH groups of GO into –OH and H_2O, and GO becomes RGO. Meanwhile, Cu(OH) is dehydrated under hydrothermal conditions to form Cu_2O and H_2O. The possible reactions involved in the hydrothermal process are summarized in Eqs. (1)-(4).

$$Cu + H_2O \leftrightarrow Cu(OH) + H^* \quad (1)$$

$$H^* + H^* \rightarrow H_2 \quad (2)$$

$$GO + H^*/H_2 \rightarrow RGO + H_2O \quad (3)$$

$$2\,Cu(OH) \rightarrow Cu_2O + H_2O \quad (4)$$

The RGO/Cu_2O/Cu composites thus obtained can be directly used as electrodes in supercapacitors, and their performance was assessed using cyclic voltammetry (CV), chronopotentiometry, and electrochemical impedance spectroscopy (EIS). CV has been considered to be a suitable tool for estimating the difference between the non-Faradaic and Faradaic reactions. CV measurements were conducted using a 3-electrode cell, in which Pt foil, SCE, and as-synthesized RGO/Cu_2O/Cu composites were used as the auxiliary electrode, reference electrode, and working electrode, respectively. Fig.7a shows the CV curves obtained from the RGO/Cu_2O/Cu composites with a scan rate of 20 mV s^{-1}, and Fig.7b shows the CV curves of the

RGO/Cu_2O/Cu-200 sample obtained with different scan rates in the range of 5 mV s^{-1} to 100 mV s^{-1}. All the CV loops clearly display a pair of redox peaks, suggesting that RGO/Cu_2O/Cu composites have excellent capacitance [58, 59], which was contributed by double layer capacitors and pseudo capacitors in their structure. Furthermore, the RGO/Cu_2O/Cu-200 sample exhibits much better performance than the others (Fig.7a).

Fig.8 shows the galvanostatic charge/discharge performance of the RGO/Cu_2O composites prepared at different temperatures. The specific capacitance C_s (shown in Table 1) can be calculated, using the following equation [60]:

$$C_s = I\Delta t/\Delta V$$

Where ΔV (V) is the potential window, and I (A g^{-1}) is the discharge current density at time Δt (s).

Fig.8a and Table 1 clearly demonstrate that the capacitance obtained at current density of 1 A g^{-1} increases as the sample preparation temperature increases from 160 °C (33.3 F g^{-1}), through 180 °C (57.0 F g^{-1}), to 200 °C (98.5 F g^{-1}), but it decreases when the temperature is further increased from 200 °C (98.5 F g^{-1}), through 220 °C (73.1 F g^{-1}), to 240 °C (62.5 F g^{-1}). On increasing the current density from 1 A g^{-1} to 5 A g^{-1}, the capacitance shows the same dependence on the temperature. In addition, at least 53% capacitance was retained at 5 A g^{-1} for all RGO-containing samples in comparison with the capacitance measured at current density of 1 A g^{-1}, as shown in Table 1. For the RGO/Cu_2O/Cu-200 sample in particular, 88% capacitance (86.9 F g^{-1}) was retained when the current density was 3 A g^{-1}, and over 64%

capacitance (63.2 F g^{-1}) was still retained even when a current density of 5 A g^{-1} was applied (Fig.8b and Table 1). Therefore, the sample prepared at 200 °C has the best performance, i.e. excellent discharge efficiency and electrochemically dynamic properties [61], which are consistent with the CV results.

Similar to a previous report, a pair of small plateaus with starting potential and ending potential close to those in the CV curves (Fig.7) appears in the charging–discharging curves (Fig.8b), indicating the existence of redox reactions during the charging–discharging process [62]. The plateau during the charging process lasts longer than the discharging, resulting in a low coulombic efficiency. A similar coulombic efficiency was also reported in the case of CuO [63], which is attributed to the inevitable transformation of cupric oxide into hydroxide in an alkaline solution [64, 65]. In addition, the charging/discharging voltage is significantly high for samples prepared at 220 °C and 240 °C. This could be attributed to the poor coating of relatively big Cu_2O particles by RGO at high temperature, which leads to low conductivity of the composites. The cyclability of the Cu_2O/RGO/Cu-200 electrode was also assessed by 1000 continuous charging/discharging measurements at a current density of 1 A g^{-1} within the potential range of -0.8–0 V (Fig. 9a). Although a clear drop occurred in the initial cycles, the specific capacitance is very stable after 150 cycles. The Coulombic efficiency increases from 40% to 100% with the cycles increasing to 350 cycles, and then keeps constant from 350 cycles to 1000 cycles (Fig. 9a).

Fig. 9b presents the Nyquist plots of various RGO/Cu_2O/Cu electrodes in the

frequency range of 10 kHz to 0.01 Hz in 1 M KOH aqueous solution. Each impedance spectrum has a semicircular arc and a straight line for all the RGO/Cu_2O/Cu and Cu_2O/Cu composites. The magnitude of the equivalent series resistance (ESR), determining the rate that the electrochemical supercapacitors (ESCs) can be charged/discharged, which is an important factor in determining the power density of ESCs, is obtained from the x-intercept of the Nyquist plot. Obviously, the RGO/Cu_2O/Cu-200 composite has the smallest ESR value (0.35 Ω), and all the composite samples show smaller ESR values than Cu_2O/Cu. These results indicate that the as-synthesized composites, especially the RGO/Cu_2O/Cu-200, have good rate capability, which is consistent with the CV and galvanostatic charge-discharg results.

The high-frequency semicircle is ascribed to the double-layer capacitance (C_{dl}) in parallel with the charge transfer resistance (R_{ct}) at the contact interface between the electrodes and the electrolyte solution [66, 67]. The R_{ct} values for all samples are smaller than 3.0 Ω, and there is no distinct difference between them. The slope at the lower frequencies represents the diffusive resistance of the electrolyte in electrode pores and the proton diffusion in the host material. It should be a vertical line in principle, which is parallel to the imaginary axis. However, except that of RGO/Cu_2O/Cu-200 sample, the slopes of other samples distinctly deviate from the expected vertical line due to electrode inhomogeneity and the existence of a “constant phase element” [68, 69]. The large slope of the RGO/Cu_2O/Cu-200 sample suggests pure capacitive behavior and low diffusion resistance of ions in its electrode.

The excellent supercapacitor performance may be attributed to the unique

structure of the RGO/Cu_2O/Cu composites. As seen in the SEM images (Figs.5-6), a layer of RGO covered Cu_2O particles has formed on the Cu substrates during the hydrothermal process. The entangled graphene sheets interact with the Cu_2O layer underneath to form an open pore system, through which electrolyte ions can easily gain access to the surface graphene to form electrical double layers [70]. This structure leads to efficient utilization of such pseudo- and double-layer capacitors to produce electrical double layer and Faraday capacitance [71, 72]. As shown in Fig.5, only the RGO/Cu_2O/Cu-200 sample has a uniform RGO network that is well spread and in contact with the Cu_2O layer. Thus a well-defined and stable interface is formed in this sample, which facilitates the ion diffusion and electrochemical reactions.

4. Conclusions

In summary, RGO/Cu_2O composite films were successfully synthesized on the surface of copper foil substrates through an in-situ redox reaction between the GO and the Cu foil, assisted by hydrothermal treatment. Due to its unique structure (i.e. RGO layer completely covered and in good contact with the Cu_2O layer), the RGO/Cu_2O/Cu electrode prepared at 200 °C exhibited a specific capacitance of 98.5 F g^{-1} at a discharge current density of 1 A g^{-1} and 63.2 F g^{-1} at 5 A g^{-1}, respectively. The electrochemical performance of all the resultant RGO/Cu_2O/Cu composites is much better than that of Cu_2O/Cu.

Acknowledgments: Financial support was provided by the National Natural Science Foundation of China (No.20504026), the Shanghai Natural Science Foundation (No.13ZR1411900), the Shanghai Leading Academic Discipline Project (B502), and the Shanghai Key Laboratory Project (08DZ2230500). Z. Li acknowledges support from the Australian Research Council through Discovery Projects DP130102699 and DP130102274.

References

[1] P. Simon, Y. Gogotsi, Nat. Mater. 7 (2008) 845-854.

[2] K.V. Gurav, U.M. Patil, S.W. Shin, G.L. Agawane, M.P. Suryawanshi, S.M. Pawar, P.S. Patil, C.D. Lokhande, J.H. Kim, J. Alloys Compd. 573 (2013) 27-31.

[3] T. Xiao, X. Hu, B. Heng, X. Chen, W. Huang, W. Tao, H. Wang, Y. Tang, X. Tan, X. Huang, J. Alloys Compd. 549 (2013) 147-151.

[4] X. Liu, B. Qu, F. Zhu, L. Gong, L. Su, L. Zhu, J. Alloys Compd. 560 (2013) 15-19.

[5] B. Senthilkumar, K. Vijaya Sankar, C. Sanjeeviraja, R. Kalai Selvan, J. Alloys Compd. 553 (2013) 350-357.

[6] M. Kaempgen, C.K. Chan, J. Ma, Y. Cui, G. Gruner, Nano Lett. 9 (2009) 1872-1876.

[7] C.C. Hu, W.C. Chen, K.H. Chang, J. Electrochem. Soc. 151 (2004) A281-A290.

[8] C.C. Hu, K.H. Chang, M.C. Lin, Y.T. Wu, Nano Lett. 6 (2006) 2690-2695.

[9] T.P. Gujar, V.R. Shinde, C.D. Lokhande, W.Y. Kim, K.D. Jung, O.S. Joo, Electrochem. Commun. 9 (2007) 504-510.

[10] Z. Song, W. Liu, M. Zhao, Y. Zhang, G. Liu, C. Yu, J. Qiu, J. Alloys Compd. 560 (2013) 151-155.

[11] J.H. Shin, H.M. Park, J.Y. Song J. Alloys Compd. 551 (2013) 451-455.

[12] A. Ramadoss, S.J. Kim, J. Alloys Compd. 561 (2013) 262-267.

[13] H.B. Li, M.H. Yu, F.X. Wang, P. Liu, Y. Liang, J. Xiao, C.X. Wang, Y.X. Tong, G.W. Yang, , Nat. Commun. 4 (2013) 1894.

[14] D.P. Dubal, D.S. Dhawale, R.R. Salunkhe, V.S. Jamdade, C.D. Lokhande, J. Alloys Compd. 492 (2010) 26-30.

[15] U.M. Patil, K.V. Gurav, V.J. Fulari, C.D. Lokhande, O.S. Joo, J. Power Sources 188 (2009) 338-342.

[16] K.S. Kim, Y. Zhao, H. Jang, S.Y. Lee, J.M. Kim, K.S. Kim, J.H. Ahn, P. Kim, J.Y. Choi, B. H. Hong, Nature 457 (2009) 706-710.

[17] C. Lee, X. Wei, J.W. Kysar, J. Hone, Science 321 (2008) 385-388.

[18] E.W. Hill, A.K. Geim, K.Novoselov, F. Schedin, P. Blake, Magnetics, IEEE Trans. Magn. 42 (2006) 2694-2696.

[19] N. Tombros, C. Jozsa, M. Popinciuc, H.T. Jonkman, B.J. van Wees, Nature 448 (2007) 571-574.

[20] Z. Wang, C. Ma, H. Wang, Z. Liu, Z. Hao, J. Alloys Compd. 552 (2013) 486-491.

[21] C. Liang, M. Gao, H. Pan, Y. Liu, M. Yan J. Alloys Compd. 575 (2013) 246-256.

[22] L.Q. Lu, Y. Wang, Electrochem. Commun. 14 (2012) 82-85.

[23] W. Zhou, J. Zhu, C. Cheng, J. Liu, H. Yang, C. Cong, C. Guan, X. Jia, H.J. Fan, Q. Yan, C.M. Li, T. Yu, Energy Environ. Sci. 4 (2011) 4954-4961.

[24] S.D. Seo, D.H. Lee, J.C. Kim, G.H. Lee, D.W. Kim, Ceram. Int. 39 (2013) 1749-1755.

[25] J. Zhou, L. Ma, H. Song, B. Wu, X. Chen, Electrochem. Commun. 13 (2011) 1357-1360.

[26] J.W. Ko, S.W. Kim, J. Hong, J. Ryu, K. Kang, C.B. Park, Green Chem. 14 (2012) 2391-2394.

[27] L.Q. Lu, Y. Wang, J. Mater. Chem. 21 (2011) 17916-17921.

[28] B. Wang, X.L. Wu, C.Y. Shu, Y.G. Guo, C.R. Wang, J. Mater. Chem. 20 (2010) 10661-10664.

[29] A.K. Rai, L.T. Anh, J. Gim, V. Mathew, J. Kang, B.J. Paul, N.K. Singh, J. Song, J. Kim, J.

Power Sources, 244 (2013) 435-441.

[30] Y.J. Mai, X.L. Wang, J.Y. Xiang, Y.Q. Qiao, D. Zhang, C.D. Gu, J.P. Tu, Electrochim. Acta 56 (2011) 2306-2311.

[31] K.H. Kim, D.W. Jung, V.H. Pham, J.S. Chung, B.S. Kong, J.K. Lee, K. Kim, E.S. Oh, Electrochim. Acta 69 (2012) 358-363.

[32] W. Liu, G. Chen, G. He, W. Zhang, J. Nanopart. Res. 13 (2011) 2705-2713.

[33] Y. Zhang, X. Wang, L. Zeng, S. Song, D. Liu, Dalton Trans. 41 (2012) 4316-4319.

[34] C. Xu, X. Wang, L. Yang, Y. Wu, J. Solid State Chem. 182 (2009) 2486-2490.

[35] B. Li, H. Cao, G. Yin, Y. Lu, J. Yin, J. Mater. Chem. 21 (2011) 10645-10648.

[36] A. Pendashteh, M.F. Mousavi, M.S. Rahmanifar, Electrochim. Acta 88 (2013) 347-357.

[37] B. Zhao, P. Liu, H. Zhuang, Z. Jiao, T. Fang, W. Xu, B. Lu, Y. Jiang, J. Mater. Chem. A 1 (2013) 367-373.

[38] F. Zhang, Y. Li, Y.e. Gu, Z. Wang, C. Wang, Microchim. Acta 173 (2011) 103-109.

[39] Y. Qian, F. Ye, J. Xu, Z.G. Le, Int. J. Electrochem. Sci. 7 (2012) 10063-10073.

[40] W.S. Hummers, R.E. Offeman, J. Am. Chem. Soc. 80 (1958) 1339-1339.

[41] Y. Xu, H. Bai, G. Lu, C. Li, G. Shi, J. Am. Chem. Soc. 130 (2008) 5856-5857.

[42] A. Lamberti, M. Destro, S. Bianco, M. Quaglio, A. Chiodoni, C. F. Pirri, C. Gerbaldi, Electrochim. Acta 70 (2012) 62-68.

[43] H.K. Jeong, Y.P. Lee, R.J. Lahaye, M.H. Park, K.H. An, I.J. Kim, C.W. Yang, C.Y. Park, R.S. Ruoff, Y.H. Lee, J. Am. Chem. Soc. 130 (2008) 1362-1366.

[44] Y. Xu, H. Bai, G. Lu, C. Li, G. Shi, J. Am. Chem. Soc. 130 (2008) 5856-5857.

[45] S. Deng, V. Tjoa, H.M. Fan, H.R. Tan, D.C. Sayle, M. Olivo, S. Mhaisalkar, J. Wei, C.H.

Sow, J. Am. Chem. Soc. 134 (2012) 4905-4917.

[46] C. Hou, H. Quan, Y. Duan, Q. Zhang, H. Wang, Y. Li, Nanoscale 5 (2013) 1227-1232.

[47] D.C. Elias, R.R. Nair, T.M.G. Mohiuddin, S.V. Morozov, P. Blake, M.P. Halsall, A.C. Ferrari, D.W. Boukhvalov, M.I. Katsnelson, A.K. Geim, K.S. Novoselov, Science 323 (2009) 610-613.

[48] S.Z. Zu, B.H. Han, J. Phys. Chem. C 113 (2009) 13651-13657.

[49] S. Pei, H.M. Cheng, Carbon 50 (2012) 3210-3228.

[50] A.C. Ferrari, J.C. Meyer, V. Scardaci, C. Casiraghi, M. Lazzeri, F. Mauri, S. Piscanec, D. Jiang, K.S. Novoselov, S. Roth, A.K. Geim, Phys. Rev. Lett. 97 (2006) 187401.

[51] Y. Qi, J.R. Eskelsen, U. Mazur, K.W. Hipps, Langmuir 28 (2012) 3489-3493.

[52] J.N. Nian, C.C. Tsai, P.C. Lin, H. Teng, J. Electrochem. Soc. 156 (2009) H567-H573.

[53] T. Ghodselahi, M.A. Vesaghi, A. Shafiekhani, A. Baghizadeh, M. Lameii, Appl. Surf. Sci. 255 (2008) 2730-2734.

[54] P. Grez, F. Herrera, G. Riveros, A. Ramírez, R. Henríquez, E. Dalchiele, R. Schrebler, phys. status solidi A 209 (2012) 2470-2475.

[55] J.Y. Park, Y.S. Jung, J. Cho, W.K. Choi, Appl. Surf. Sci. 252 (2006) 5877-5891.

[56] Y. Bai, R.B. Rakhi, W. Chen, H.N. Alshareef, J. Power Sources 233 (2013) 313-319.

[57] T. Lu, Y. Zhang, H. Li, L. Pan, Y. Li, Z. Sun, Electrochim. Acta 55 (2010) 4170-4173.

[58] Y. Zhang, H. Li, L. Pan, T. Lu, Z. Sun, J. Electroanal. Chem. 634 (2009) 68-71.

[59] Y. Wang, Z. Shi, Y. Huang, Y. Ma, C. Wang, M. Chen, Y. Chen, J. Phys. Chem. C 113 (2009) 13103-13107.

[60] Y.M. Chen, J.H. Cai, Y.S. Huang, K.Y. Lee, D.S. Tsai, Nanotechnology 22 (2011) 115706.

[61] T. Lu, L. Pan, H. Li, G. Zhu, T. Lv, X. Liu, Z. Sun, T. Chen, D.H.C. Chua, J. Alloys Compd. 509 (2011) 5488-5492.

[62] W. Zhang, F. Liu, Q. Li, Q. Shou, J. Cheng, L. Zhang, B.J. Nelson, X. Zhang, Phys. Chem. Chem. Phys. 14 (2012) 16331-16337.

[63] A. Pendashteh, M.F. Mousavi, M.S. Rahmanifar, Electrochim. Acta 88 (2013) 347-357.

[64] G.L. Wang, J.C. Huang, S.L. Chen, Y.Y. Gao, D.X. Cao, J. Power Sources 196 (2011) 5756-5760.

[65] R. Bogdanowicz, J. Ryl, K. Darowicki, B.B. Kosmowski, J. Solid State Electrochem. 13 (2009) 1639-1644.

[66] X.Z. Wang, M.G. Li, Y.W. Chen, R.M. Cheng, S.M. Huang, L.K. Pan, Z. Sun, Appl. Phys. Lett. 89 (2006) 053127-053123.

[67] M. Zhi, A. Manivannan, F. Meng, N. Wu, J. Power Sources 208 (2012) 345-353.

[68] Y. Gao, L. Pan, H. Li, Y. Zhang, Z. Zhang, Y. Chen, Z. Sun, Thin Solid Films 517 (2009) 1616-1619.

[69] G.J. Brug, M. Sluyters-Rehbach, J.H. Sluyters, A. Hemelin, J. Electroanal. Chem. 181 (1984) 245-266.

[70] W. Lv, D.M. Tang, Y.B. He, C.H. You, Z.Q. Shi, X.C. Chen, C.M. Chen, P.X. Hou, C. Liu, Q.H. Yang, ACS Nano 3 (2009) 3730-3736.

[71] Z.S. Wu, W. Ren, D.W. Wang, F. Li, B. Liu, H.M. Cheng, ACS Nano 4 (2010) 5835-5842.

[72] Z. Fan, J. Yan, L. Zhi, Q. Zhang, T. Wei, J. Feng, M. Zhang, W. Qian, F. Wei, Adv. Mater. 22 (2010) 3723-3728.

Scheme and Figure captions

Scheme 1. Schematic illustration of the synthesis of RGO/Cu_2O/Cu in polytetrafluoroethylene (PTFE, Teflon®) lined autoclave.

Fig.1 XRD patterns of RGO/Cu_2O/Cu-160, RGO/Cu_2O/Cu-180, RGO/Cu_2O/Cu-200, RGO/Cu_2O/Cu-220, RGO/Cu_2O/Cu-240, and Cu foil and pure RGO prepared by the hydrothermal method at 200°C for 24 h.

Fig.2 FT-IR spectra of RGO/Cu_2O/Cu-160, RGO/Cu_2O/Cu-180, RGO/Cu_2O/Cu-200, RGO/Cu_2O/Cu-220, RGO/Cu_2O/Cu-240, and GO.

Fig.3 Raman spectra of RGO/Cu_2O/Cu-160, RGO/Cu_2O/Cu-180, RGO/Cu_2O/Cu-200, RGO/Cu_2O/Cu-220, RGO/Cu_2O/Cu-240, pure RGO prepared by hydrothermal treatment at 200 °C for 24 h, and GO.

Fig.4 XPS spectra of RGO/Cu_2O/Cu-160, RGO/Cu_2O/Cu-180, RGO/Cu_2O/Cu-200, RGO/Cu_2O/Cu-220, RGO/Cu_2O/Cu-240, pure RGO prepared by hydrothermal treatment at 200 °C for 24 h, and GO: C 1s peaks of (a) GO, (b) RGO after hydrothermal treatment, and (c) RGO/Cu_2O/Cu-200; (d) survey spectra of all samples; (e) Cu $2p_{3/2}$ and Cu $2p_{1/2}$ peaks of RGO/Cu_2O/Cu-200 and Cu foil; (f) Cu LMM X-ray induced Auger peaks of RGO/Cu_2O/Cu-200 and copper foil.

Fig.5 FESEM images of (a) RGO/Cu_2O/Cu-200, (b) Cu foil after hydrothermal treatment, (c) tilted view of RGO/Cu_2O/Cu-200, and (d) pure graphene hydrothermally prepared at 200 °C.

Fig.6 FESEM images of surface and tilted views of (a-b) RGO/Cu_2O/Cu-160, (c-d)

RGO/Cu_2O/Cu-180, (e-f) RGO/Cu_2O/Cu-220, and (g-h) RGO/Cu_2O/Cu-240.

Fig.7 Cyclic voltammograms of (a) RGO/Cu_2O/Cu-160, -180, -200, -220, and -240 at scan rate = 20 mV/s; and (b) RGO/Cu_2O/Cu-200 electrode at different scan rates in 1 M KOH electrolyte.

Fig.8 Galvanostatic charging/discharging curves of (a) RGO/Cu_2O/Cu-160, -180, -200, -220, and -240 at a current density of 1 A g^{-1}; and (b) RGO/Cu_2O/Cu-200 electrode at various current densities in 1 M KOH electrolyte.

Fig.9 (a) Cycling performance and coulombic efficiency of RGO/Cu_2O/Cu-200 electrode at a current density of 1 A·g^{-1} in 1 M KOH electrolyte. (b) Nyquist plots of experimental impedance data for RGO/Cu_2O/Cu-160, -180, -200, -220, and -240 nanocomposite electrodes and Cu_2O/Cu-200 electrode in the frequency range of 100 kHz to 0.01 Hz. The inset contains the magnified plots at high frequency.

Table 1. Specific capacitance of RGO/Cu_2O/Cu composites prepared at 160, 180, 200, 220, and 240 °C at different current densities.

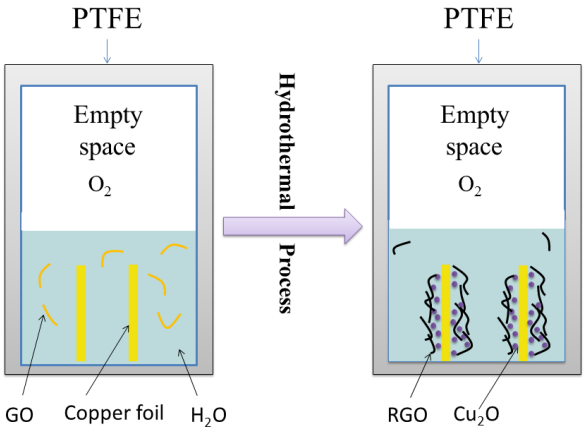
PTFE
Empty space
O_2
GO
Copper foil
H_2O
Hydrothermal Process
PTFE
Empty space
O_2
RGO
Cu_2O

Scheme 1

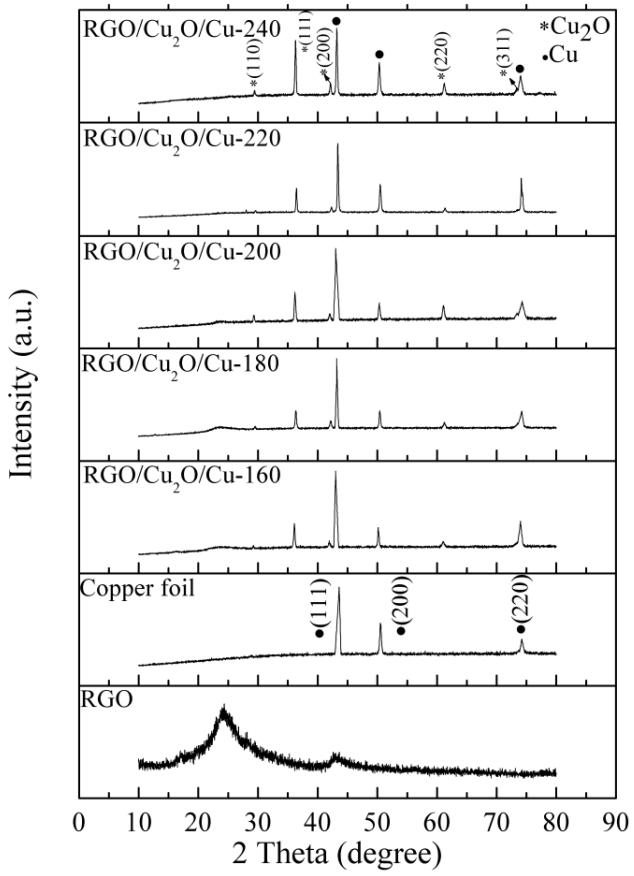
RGO/Cu2O/Cu-240
*Cu2O
•Cu
*(110)
*(111)
•(200)
*(220)
*(311)
RGO/Cu2O/Cu-220
RGO/Cu2O/Cu-200
RGO/Cu2O/Cu-180
RGO/Cu2O/Cu-160
Copper foil
•(111)
•(200)
•(220)
RGO
Intensity (a.u.)
0 10 20 30 40 50 60 70 80 90
2 Theta (degree)

Fig. 1

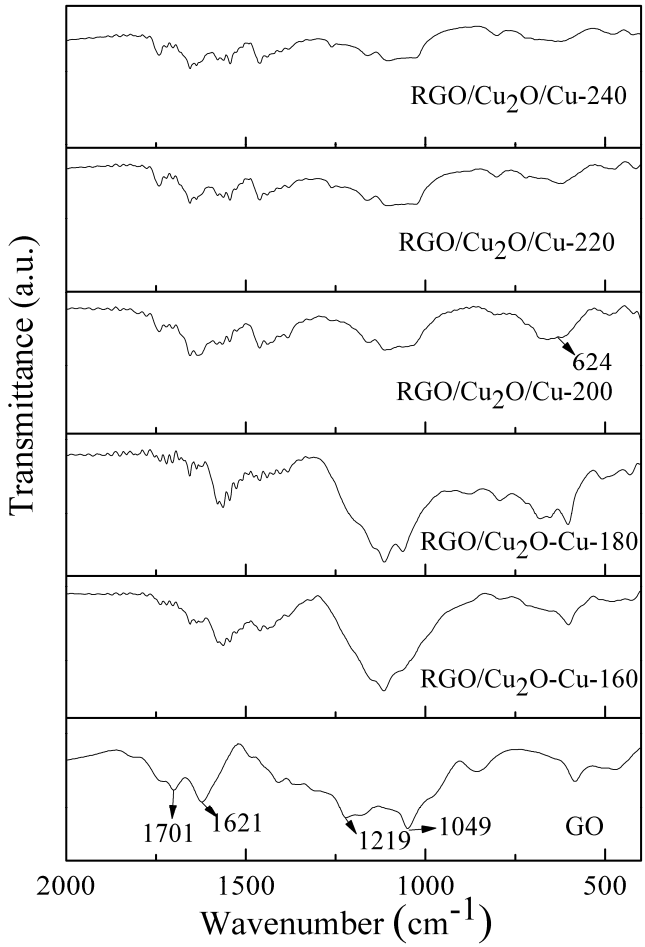
RGO/Cu2O/Cu-240
RGO/Cu2O/Cu-220
624
RGO/Cu2O/Cu-200
RGO/Cu2O-Cu-180
RGO/Cu2O-Cu-160
1701
1621
1219
1049
GO
Transmittance (a.u.)
2000
1500
1000
500
Wavenumber (cm-1)

Fig. 2

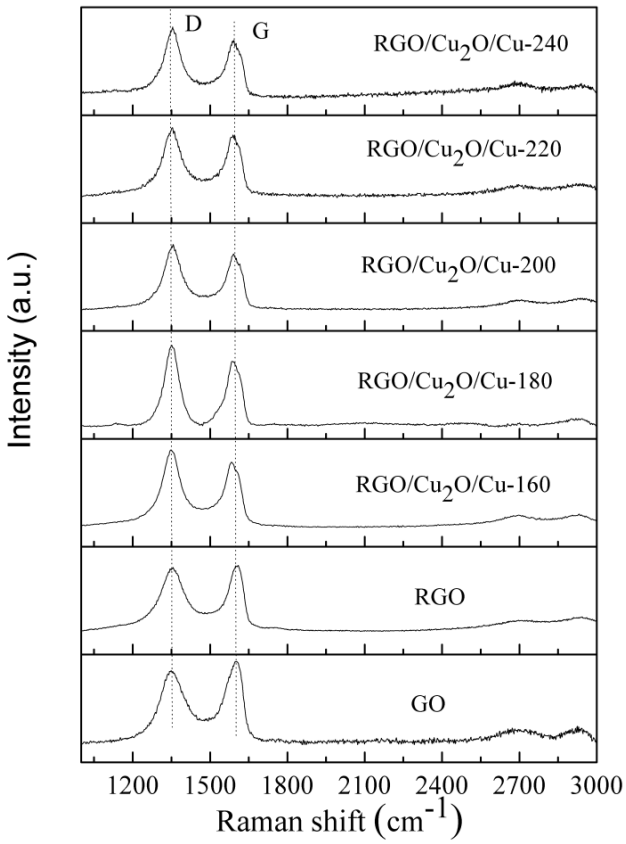
D
G
RGO/Cu2O/Cu-240
RGO/Cu2O/Cu-220
RGO/Cu2O/Cu-200
RGO/Cu2O/Cu-180
RGO/Cu2O/Cu-160
RGO
GO
Intensity (a.u.)
1200
1500
1800
2100
2400
2700
3000
Raman shift (cm-1)

Fig. 3

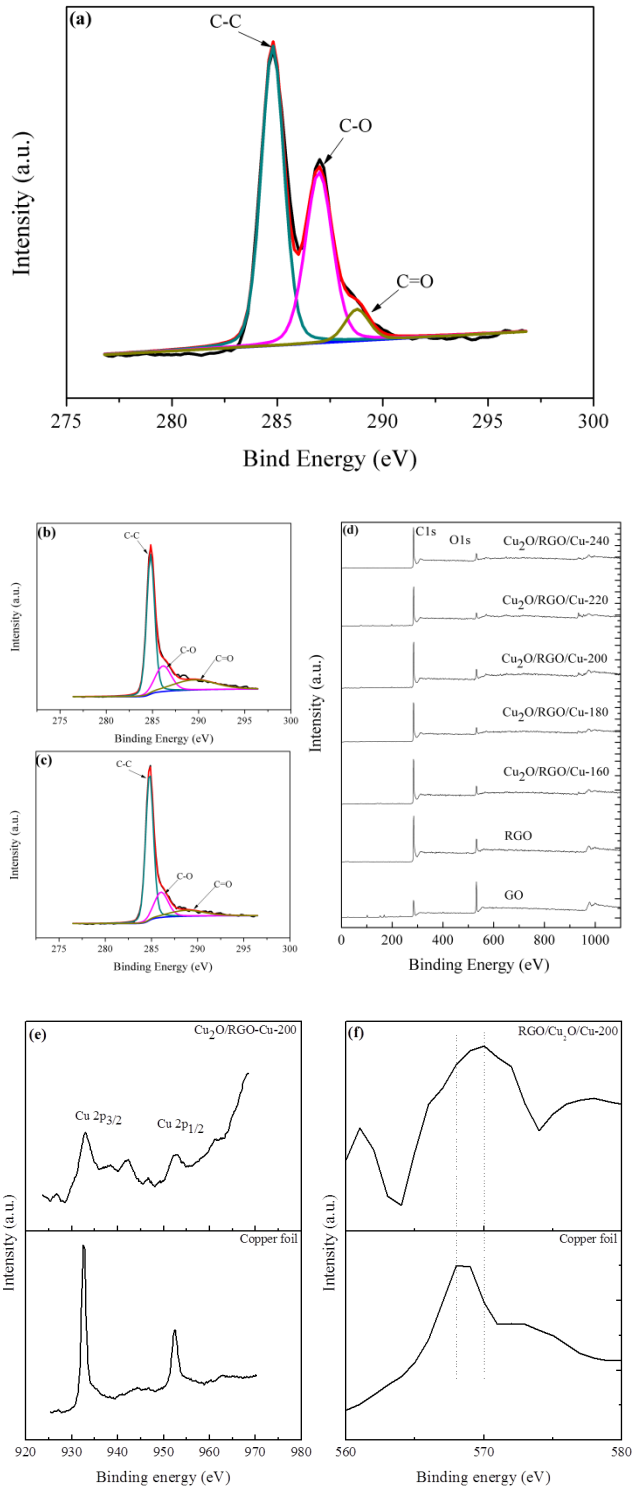
(a)
C-C
C-O
C=O
Intensity (a.u.)
275
280
285
290
295
300
Bind Energy (eV)
(b)
C-C
C-O
C=O
Intensity (a.u.)
Binding Energy (eV)
(c)
C-C
C-O
C=O
Intensity (a.u.)
Binding Energy (eV)
(d)
C1s
O1s
Cu2O/RGO/Cu-240
Cu2O/RGO/Cu-220
Cu2O/RGO/Cu-200
Cu2O/RGO/Cu-180
Cu2O/RGO/Cu-160
RGO
GO
Intensity (a.u.)
0
200
400
600
800
1000
Binding Energy (eV)
(e)
Cu2O/RGO-Cu-200
Cu 2p3/2
Cu 2p1/2
Copper foil
Intensity (a.u.)
920
930
940
950
960
970
980
Binding energy (eV)
(f)
RGO/Cu2O/Cu-200
Copper foil
Intensity (a.u.)
560
570
580
Binding energy (eV)

Fig. 4

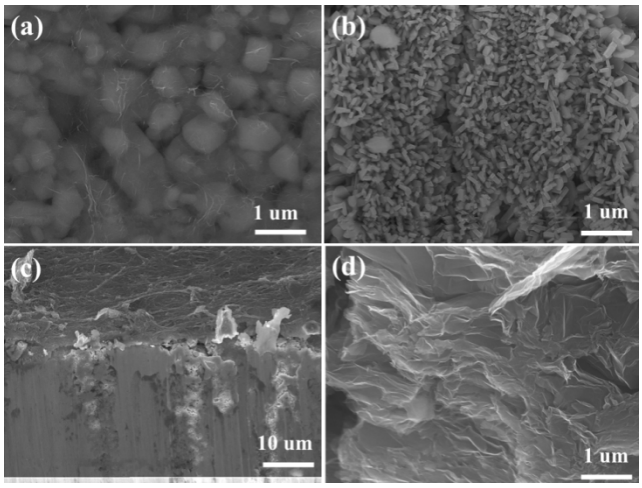

Fig. 5

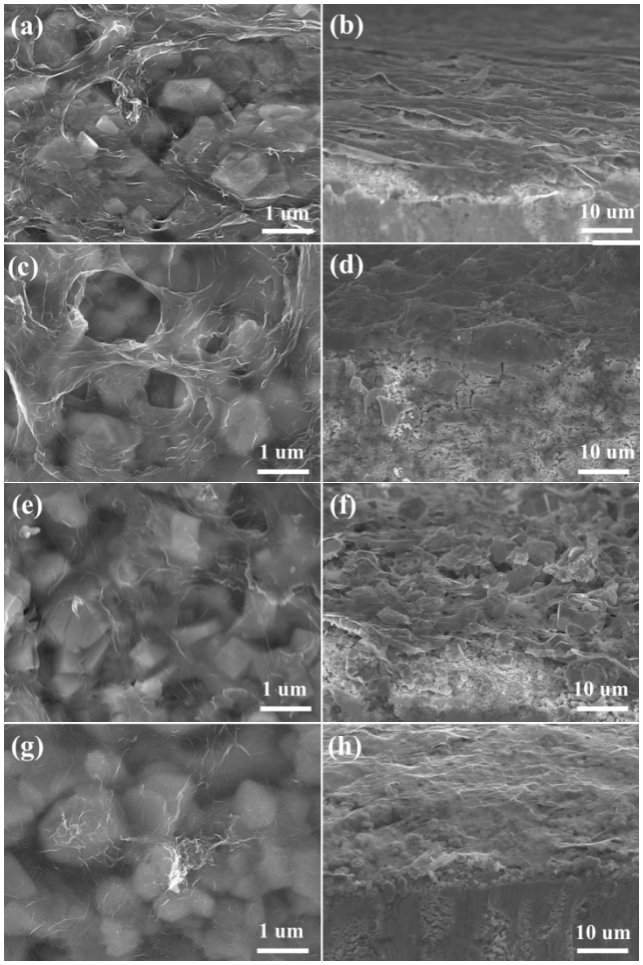

Fig. 6

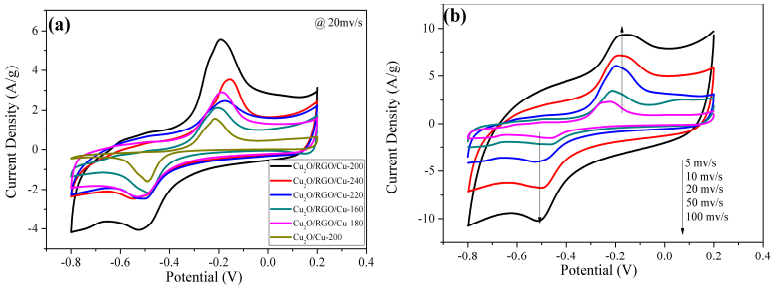
(a)
@ 20mv/s
Current Density (A/g)
Potential (V)
Cu2O/RGO/Cu-200
Cu2O/RGO/Cu-240
Cu2O/RGO/Cu-220
Cu2O/RGO/Cu-160
Cu2O/RGO/Cu 180
Cu2O/Cu-200
(b)
Current Density (A/g)
Potential (V)
5 mv/s
10 mv/s
20 mv/s
50 mv/s
100 mv/s

Fig. 7

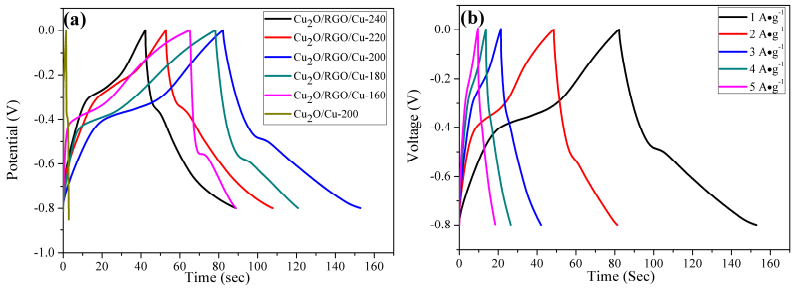
(a)
Cu2O/RGO/Cu-240
Cu2O/RGO/Cu-220
Cu2O/RGO/Cu-200
Cu2O/RGO/Cu-180
Cu2O/RGO/Cu-160
Cu2O/Cu-200
Potential (V)
Time (sec)
(b)
1 A•g-1
2 A•g-1
3 A•g-1
4 A•g-1
5 A•g-1
Voltage (V)
Time (Sec)

Fig. 8

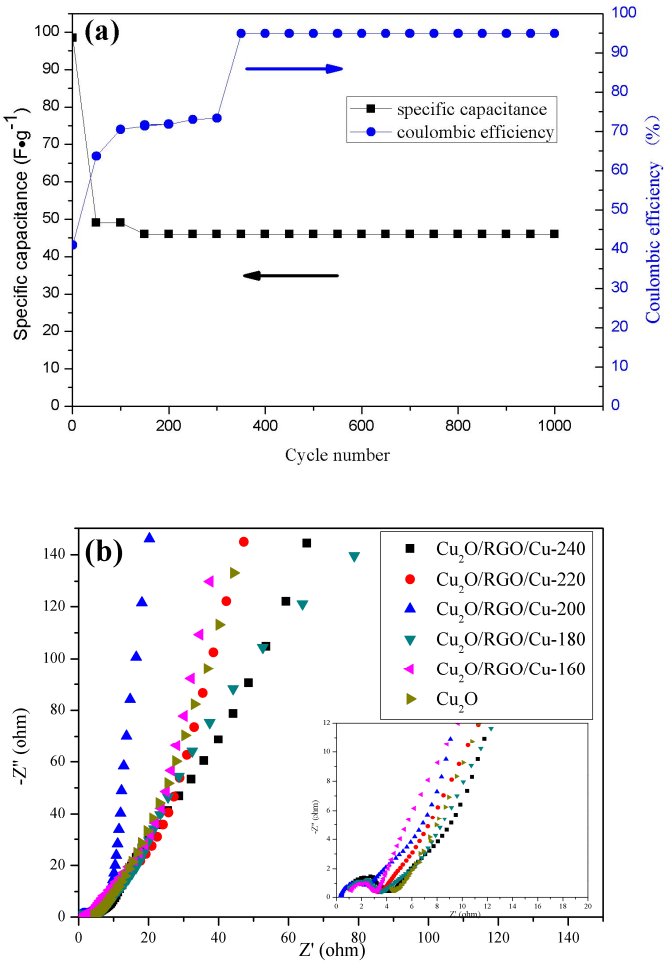
(a)
specific capacitance
coulombic efficiency
Specific capacitance (F•g-1)
Coulombic efficiency (%)
Cycle number
(b)
Cu2O/RGO/Cu-240
Cu2O/RGO/Cu-220
Cu2O/RGO/Cu-200
Cu2O/RGO/Cu-180
Cu2O/RGO/Cu-160
Cu2O
-Z'' (ohm)
Z' (ohm)

Fig.9

Table 1

Sample	Specific capacitance ($F\ g^{-1}$)				
	$1Ag^{-1}$	$2Ag^{-1}$	$3Ag^{-1}$	$4Ag^{-1}$	$5Ag^{-1}$
RGO/Cu_2O/Cu-160	33.3	18.9	26.2	20.5	18.7
RGO/Cu_2O/Cu-180	57.0	50.7	42.6	41.8	40.6
RGO/Cu_2O/Cu-200	98.5	91.9	86.9	71.8	63.2
RGO/Cu_2O/Cu-220	73.1	61.7	51.5	44.5	40.1
RGO/Cu_2O/Cu-240	62.5	60.3	47.3	41.4	33.2